ACS chemical biology

Articles

Cite This: ACS Chem. Biol. XXXX, XXX, XXX−XXX

pubs.acs.org/acschemicalbiology

New Molecular Scaffolds for Fluorescent Voltage Indicators

Steven C. Boggess,[†] Shivaani S. Gandhi,[†] Brian A. Siemons,[‡,§] Nathaniel Huebsch,[‡,§,#] Kevin E. Healy,[‡,§] and Evan W. Miller*[,†,∥,⊥]

[†]Departments of Chemistry, [‡]Bioengineering, [§]Materials Science & Engineering, and [∥]Molecular & Cell Biology and [⊥]Helen Wills Neuroscience Institute, University of California, Berkeley, California 94720, United States

Supporting Information

ABSTRACT: The ability to non-invasively monitor membrane potential dynamics in excitable cells like neurons and cardiomyocytes promises to revolutionize our understanding of the physiology and pathology of the brain and heart. Here, we report the design, synthesis, and application of a new class of fluorescent voltage indicators that make use of a fluorene-based molecular wire as a voltage-sensing domain to provide fast and sensitive measurements of membrane potential in both mammalian neurons and human-derived cardiomyocytes. We show that the best of the new probes, fluorene VoltageFluor 2 (fVF 2), readily reports on action potentials in mammalian neurons, detects perturbations to the cardiac action potential waveform in human induced pluripotent stem cell-derived cardiomyocytes, shows a substantial decrease in phototoxicity compared to existing molecular wire-based indicators, and can monitor cardiac action potentials for extended periods of time. Together, our results demonstrate the generalizability of a molecular wire approach to voltage sensing and highlight the utility of fVF 2 for interrogating membrane potential dynamics.

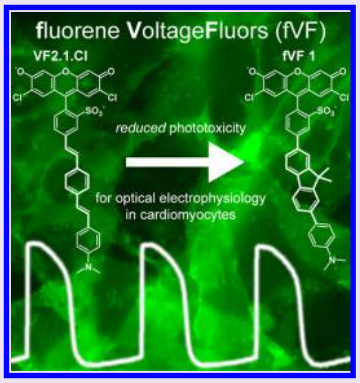

Optical methods for measuring biochemical and biophysical events in living cells provide a powerful approach for monitoring cellular physiology in a non-invasive and high-throughput manner. The success of such light-based ventures depends critically on the ability to design and construct molecules that change their optical properties, for example, color, fluorescence intensity, or lifetime, in response to changes in the cellular environment.[1] Fluorescence microscopy is one of the most commonly used modalities because it is operationally simple, the instrumentation is widely available, and an ever-growing library of small molecule fluorescent indicators exists to probe the dynamics of a host of cellular analytes, properties, and structures.[2−5] Of particular interest is the plasma membrane. Changes in the electrochemical potential across the lipid bilayer profoundly shape cellular physiology. Excitable cells employ a consortium of ion channels both to maintain tight control over their membrane potential (V_m) and to initiate and propagate rapid changes in V_m. Rapid changes in V_m such as an action potential (AP) drive the unique physiology of excitable cells like neurons and cardiomyocytes. In neurons, APs evoke the release of the neurotransmitter into the synaptic cleft, and in heart tissue, waves of APs coordinate contraction and maintain regular rhythm. Disruption of the frequency, timing, and/or shape of APs is linked to serious human diseases ranging from epilepsy to long QT syndrome. Because of the importance of V_m to both health and disease, robust methods for optically monitoring the membrane potential remain a critical complement to more traditional approaches. The gold standard for measuring V_m and APs in live cells is electrophysiology: direct determination of V_m through the physical interaction between the cell of interest and an electrode. Electrophysiology is highly invasive, low-throughput, and difficult to interpret in samples like cardiac tissue or cardiomyocyte monolayers, where electrical coupling between cells confounds single-cell measurement. Optical recording of the membrane potential using voltage-sensitive fluorescent indicators provides an attractive alternative to probing V_m and AP dynamics in multiple cells, in monolayers, or three-dimensional tissue.[6]

Recently, we initiated a program to develop a new class of voltage-sensitive fluorescent indicators that utilize photoinduced electron transfer (PeT) as a rapid trigger to sense changes in V_m.[7,8] These small molecule voltage-sensitive fluorophores, or VoltageFluors (VF dyes), combine a xanthene-based dye as a fluorescent reporter and a conjugated molecular wire that localizes the indicator to the cell membrane and facilitates PeT from an electron-rich aniline donor to the fluorophore within the low-dielectric environment of the lipid bilayer. Phenylene-vinylene (PV)-based conjugated molecular wires (Scheme 1, VF2.1.Cl)[9,10] are attractive because of their exceptionally low electron transfer attenuation values in donor−bridge−acceptor (DBA) systems (β = 0.04 Å^{-1}).[11,12] Within a PV wire framework, voltage sensitivity can be improved by altering the redox potentials of the fluorophore electron acceptor and the aniline electron donor.[13] Additionally, fluorophores such as rhodamine[9] and silicon-rhodamine[10] can be substituted for fluorescein, after some adjustment to the identity of the aniline donor. To date,

Received: November 1, 2018
Accepted: January 24, 2019

DOI: 10.1021/acschembio.8b00978
ACS Chem. Biol. XXXX, XXX, XXX−XXX

Scheme 1. Synthesis of Fluorene VoltageFluor Dyes (fVF dyes)

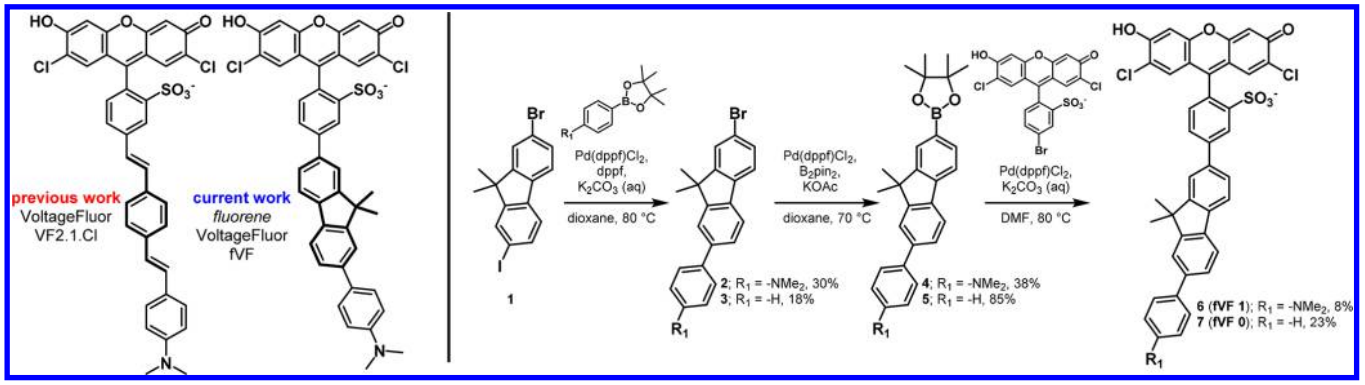

Scheme 2. Synthesis of Electron-Rich Fluorene VoltageFluor Dyes

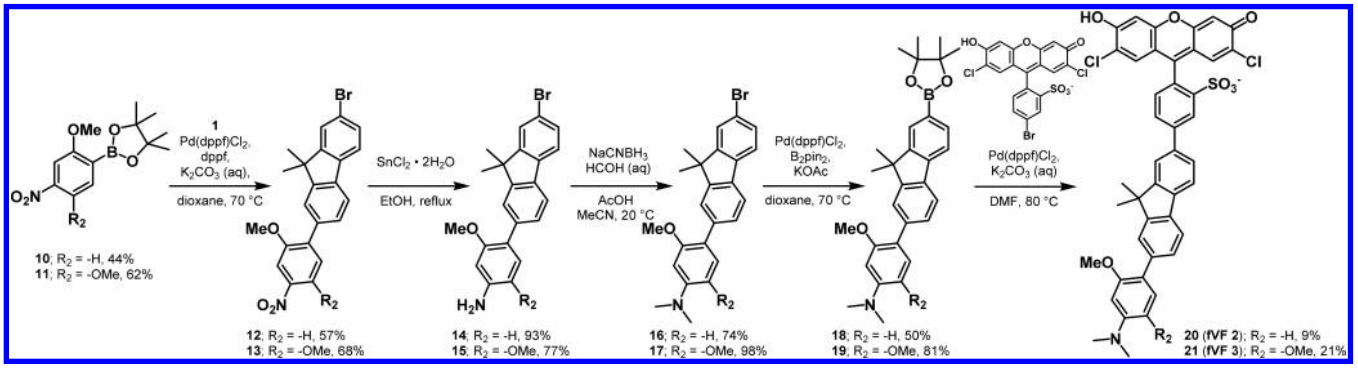

we have not explored alterations to the identity of the molecular wire component of PeT-based voltage indicators. Now, we present a new class of PeT-based voltage-sensitive fluorescent indicators that use a 9,9-dimethyl-9*H*-fluorene monomer in place of the canonical 1,4-divinylbenzene moiety (Scheme 1). In other DBA scaffolds, 2,7-oligofluorene bridges effectively facilitate electron transfer across large distances and demonstrate low β values (0.09 Å^{-1}) comparable to values for PV wires (0.04 Å^{-1}).[14] Because β values depend both on the identity of the wire and on the donor/acceptor pair,[15,16] we wanted to explore fluorene molecular wires as a platform for optical voltage sensing, demonstrating the generalizability of a PeT-based approach to voltage sensing. We now report the design, synthesis, characterization, and application of a new series of fluorene-based VoltageFluors, or fVF dyes.

The synthesis of fluorene-based voltage indicators starts with Suzuki−Miyaura cross-coupling of bromo-iodo-fluorene **1**[17] with either boronic ester **8**[18] or phenylboronic acid, providing monomeric fluorenes **2** and **3** as bright yellow solids (Scheme 1). Attachment to a sulfonated dichlorofluorescein was achieved by Pd-catalyzed cross-coupling of a pinacol boronic ester with the terminal aryl bromide to provide **4** and **5**. Suzuki−Miyaura cross-coupling yielded voltage indicator **6** (**fVF 1**) and indicator **7** (**fVF 0**), which lacks an aniline donor (Scheme 1). For the wires with electron-rich donors [**12** and **13** (Scheme 2)], transformation of the nitro group to an aniline was performed with tin(II) chloride to yield wires **14** and **15**. This was followed by reductive amination of formaldehyde with $NaCNBH_3$ to provide alkylated wires **16** and **17**. These were prepared via a method similar to that depicted in Scheme 1 to yield electron-rich voltage indicators **20** (**fVF 2**) and **21** (**fVF 3**).

New fVF dyes have a λ_{max} centered around 520 nm and a second major absorption band around 340 nm arising from the fluorene molecular wire (Figure 1, Figure S1, and Table 1). Each fVF dye has a maximum emission around 535 nm, indicating little ground state interaction between the fluorene-based molecular wire and xanthene chromophore. **fVF 1−3** have fluorescence quantum yields (Φ_{fl}, 0.05−0.19) that are lower than that of control indicator **fVF 0** [0.77 (Table 1)].

To measure the voltage sensitivity of these indicators, we used whole cell voltage-clamp electrophysiology in tandem with epifluoresence microscopy. By applying voltage steps ranging from 100 to −100 mV in 20 mV increments to HEK293T cells stained with fluorene voltage indicators, we observe that indicators **fVF 1−3** possess moderate sensitivity to changes in V_m. Similar to PV-based molecular wire voltage indicators, **fVF 1−3** become brighter in response to depolarizing (more positive) membrane potentials. The two most sensitive compounds, **fVF 2** and **3**, have sensitivities of 11 and 13% $\Delta F/F$ per 100 mV, respectively; however, **fVF 2** has an overall signal that was much brighter in cells, resulting in a better signal-to-noise ratio (SNR) (Figure 1, Figure S2, and Table 1). **fVF 1** is also very bright in cells but has a low SNR due to a low sensitivity (5% $\Delta F/F$). Somewhat surprisingly, the electron-deficient compound **fVF 0** [**7** (Scheme 1)] exhibits a small amount of voltage sensitivity, −0.3% $\Delta F/F$ per 100 mV, becoming less fluorescent in response to depolarizing potentials (Table 1, Figure S2, and Table 1), a behavior that is the opposite of that of every molecular wire indicator synthesized in our laboratory. We chose to characterize **fVF 2** in subsequent experiments due to its brightness and superior SNR.

fVF 2 readily detects fast changes in membrane potential in mammalian neurons. In cultured rat hippocampal neurons, **fVF**

DOI: 10.1021/acschembio.8b00978
ACS Chem. Biol. XXXX, XXX, XXX−XXX

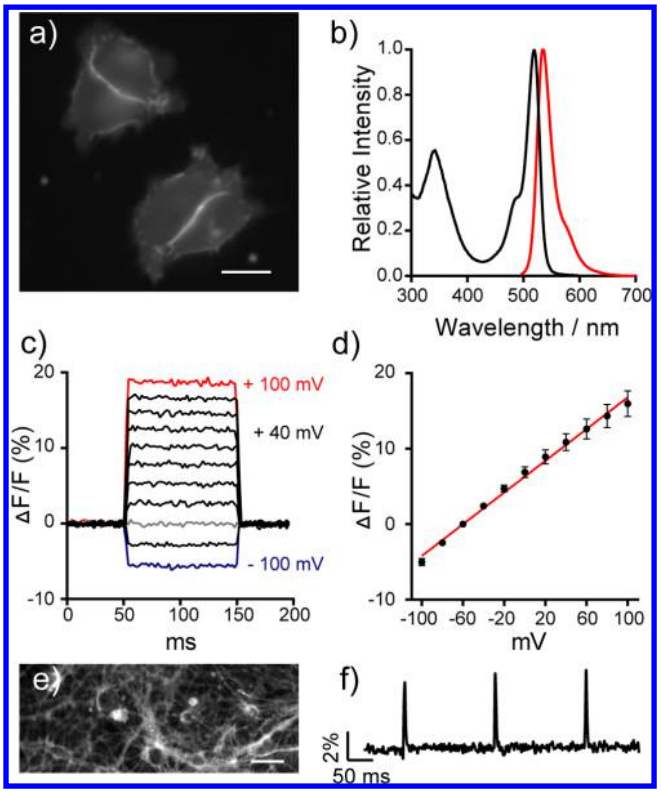

Figure 1. Characterization of fluorene VoltageFluor 2 (**fVF 2**). (a) Live cell fluorescence microscopy image of **fVF 2** in HEK cells. The scale bar is 10 μm. (b) Normalized absorption and emission spectra of **fVF 2**. Spectra were acquired in phosphate-buffered saline (pH 7.2) and 0.1% sodium dodecyl sulfate. For an emission scan, excitation was provided at 485 nm. (c) Voltage sensitivity of **fVF 2** in patch-clamped HEK cells. (d) Plot of $\Delta F/F$ vs membrane potential (in millivolts) for **fVF 2**. The red line is the line of best fit. Error bars are standard errors of the mean for eight independent determinations. (e) Live cell, wide-field fluorescence images of rat hippocampal neurons stained with 500 nM **fVF 2**. The scale bar is 20 μm. (f) Representative $\Delta F/F$ plot of evoked neuronal activity of a single cell recorded optically with **fVF 2**.

2 gives clear membrane staining (Figure 1e) and faithfully records evoked action potentials with an average $\Delta F/F$ of 5.1% and SNR of 21:1 [n = 54 spikes (Figure 1f and Figure S4)]. **fVF 2** clearly resolves spontaneous activity in cultured rat hippocampal neurons (Figure S5). Despite the lower nominal voltage sensitivity of **fVF 2** relative to a first-generation VoltageFluor dye [VF2.1.Cl, 27% $\Delta F/F$ per 100 mV in HEK cells,[7] 10% $\Delta F/F$ and a SNR of 43:1 in evoked action potentials; n = 54 spikes (Figure S4)], the improved brightness of **fVF 2** relative to VF2.1.Cl [1.2 times brighter in neurons (Table S1)] makes it useful for recording action potentials in neurons. When we evaluate **fVF 2** against an electrochromic VSD with a similar voltage sensitivity, di-4-ANEPPS, we observe evoked spikes with a $\Delta F/F$ of −1% and a SNR of 15:1. However, a 5-fold higher concentration was needed to make these recordings (Figure S4 and Table S1). In addition to reporting on neuronal activity, we detect no changes to neuronal membrane properties or action potential kinetics when comparing the electrophysiological parameters of neurons in the absence or presence of fVF2 (Figure S6 and Table S2).

We sought to use **fVF 2** for optical measurements of cardiac AP waveforms to provide a holistic assessment of drug cardiotoxicity *in vitro*, a major goal of the Comprehensive *in vitro* Proarrythmic Assay (CiPA) initiative.[19−21] We cultured hiPSC-CM monolayers and tested the ability of **fVF 2** to report cardiac AP waveforms in spontaneously beating monolayers.[21−25] **fVF 2** clearly stains the sarcolemma of hiPSC-CMs and faithfully reports ventricular-like AP waveforms, showing a large increase in fluorescence just before contraction of the monolayer (Figure 2a−e). Using methods previously described,[26] we calculate the action potential duration (APD) for each AP waveform in the fluorescence trace at 70, 50, and 10% of the maximum depolarization (APD30, APD50, and APD90, respectively).[26−28] To correct for APD variation arising from the difference in beat rate from spontaneously beating monolayers, we used Fridericia's formula to provide a beat-rate corrected APD (cAPD).[28,29] From our optical measurements, we calculated cAPD90 values from 500 to 700 ms in spontaneously beating monolayers after 14 days in culture, consistent with previous reports for hiPSC-CMs.[27,30]

To demonstrate the utility of **fVF 2** for parsing the pharmacological effects of drug treatment on cardiomyocytes, we treated hiPSC cardiomyocytes with cisapride. Cisapride, formally a useful gastroprokinetic agent, was withdrawn from the U.S. market in 2000 due to its connection to torsades de pointes (TdP) induced by acquired long QT syndrome caused by blockage of K_v11.1.[31] Cisapride is also one of 12 training and calibration compounds used in the CiPA initiative.[20,32] The observation of cardiomyocyte monolayers treated acutely with cisapride results in several phenotypic alterations to cardiac AP, which can be readily detected by **fVF 2**. At a concentration of 300 nM, we saw three different manifestations of the effect of prolonged cAPD caused by I_{Kr} blockade:[33,34] an extended phase 3 (Figure 2g), a tachycardia-like train of drastically shortened APs (Figure 2h), and the appearance of early after depolarizations (EADs) (Figure 2i). K_v11.1/hERG channel blockade results in action potential prolongation (Figure 2g), which has been connected to a higher risk of TdP and higher arrhythmogenic potential. The rapid, subthreshold spiking activity may be analogous to tachycardia,[35] which was accompanied by a loss of monolayer automaticity (Figure 2h). The appearance of EADs (Figure 2i) corresponds to the

Table 1. Properties of Fluorene VoltageFluor Dyes (fVF dyes)

entry[a]	R^1	R^2	absorbance (nm)[a]	emission (nm)[a]	QY[a]	% $\Delta F/F$[b]	SNR[b]
fVF 0 (7)	-H	-H	519	535	0.77	−0.3 ± 0.03	1.9:1
fVF 1 (6)	$-N(Me)_2$	-H	519	534	0.05	4.7 ± 0.5	22:1
fVF 2 (20)	$-N(Me)_2$	-H	520	535	0.07	10.5 ± 0.8	39:1
fVF 3 (21)	$-N(Me)_2$	-OMe	520	535	0.19	12.2 ± 1.6	13:1

[a]Measured in phosphate-buffered saline and 0.1% sodium dodecyl sulfate (pH 7.2). [b]Per 100 mV. Recorded in HEK 293T cells at an optical sampling rate of 0.5 kHz.

DOI: 10.1021/acschembio.8b00978
ACS Chem. Biol. XXXX, XXX, XXX−XXX

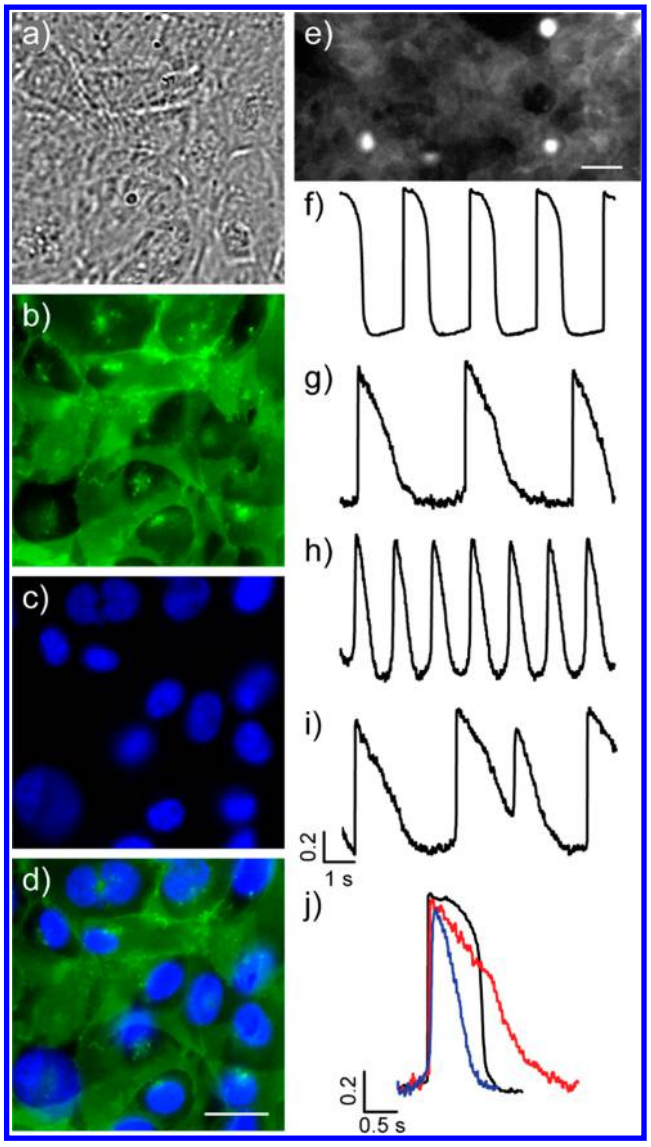

Figure 2. Fluorene VoltageFluor 2 (**fVF 2**) reliably reports on cardiac action potential (cAP) dynamics in human induced pluripotent stem cell-derived cardiomyocytes (hiPSC-CMs). (a) Bright field. (b) Membrane localization of **fVF 2** (1 μM) in hiPSC-CM monolayers. (c) Hoescht 33342 nuclear stain. (d) Merge of membrane and nuclear stains. The scale bar is 20 μm. (e) Representative image used to acquire functional AP data. The scale bar is 10 μm. (f–i) Representative fluorescence traces acquired using 1 μM **fVF 2**. (f) Baseline measurement of a spontaneously contracting monolayer. Treatment with cisapride (300 nM) results in (g) prolonged APs, (h) shorter and more frequent APs, and (i) early after depolarizations (EADs). (j) Overlay of single APs from panels f–h to highlight observed waveform changes from cisapride treatment. The baseline trace in black shows a normal ventricular-like shape; the red trace depicts an extended AP after treatment (from panel g), and the blue trace depicts a shortened AP from a tachycardia-like phenotype (from panel h).

observed cAPD prolongation and significantly increases the risk of arrhythmia and TdP.

Monitoring the effect of potentially cardiotoxic drug relies on the ability to make stable, long-term recordings from cardiomyocytes. When using voltage-sensitive fluorescent indicators, this often requires careful titration of illumination intensity and indicator concentration to minimize phototoxicity.[35−37] Therefore, we were pleased that **fVF 2** displays lower phototoxicity in hiPSC-CMs relative to VF2.1.Cl, which itself requires a light power an order of magnitude lower than that of di-4-ANEPPS, thereby avoiding phototoxic effects.[37] Others note phototoxic effects of di-4-ANEPPS can begin within seconds of illumination.[38] We stained hiPSC-CM monolayers with either **fVF 2** or VF2.1.Cl and continuously illuminated them for 10 min and optically recorded membrane potential dynamics every minute. Despite the initial photobleach of **fVF 2** (Figure 3a and Figure S2i), the shapes of recorded action potentials (Figure 3c), SNR (Figure 3e), and action potential duration (Figure 3f,g) remain relatively constant (Figure 3c,d and Figure S7). In sharp contrast, however, VF2.1.Cl had a dramatic, detrimental impact on cardiomyocyte function. Although VF2.1.Cl initially has a high SNR compared to that of **fVF 2** (Figure 3b,e), the SNR drops quickly after the first minute of illumination (Figure 3b,e), and both action potential shape (Figure 3d) and duration (Figure 3f,g) undergo substantial and significant changes, as early as 2 min into illumination (Figure 3b,d,f,g). Even after 4 min, only subthreshold activity was recorded with VF2.1.Cl and required an automated analysis script to detect these events (Figure S7h). After 5 min, monolayers imaged with VF2.1.Cl cease to contract (Figure 3d and Figure S7). However, monolayers imaged with **fVF 2** continue to beat even after continuous illumination for 10 min (Figure 3c and Figure S7). Increasing the illumination intensity from 9 to 29 mW/mm^2 when making recordings with **fVF 2** did not alter cAPD (Figure S7l). Toxicity requires both dye and illumination, as regions of the coverslip not exposed to illumination light beat properly, in the case of **fVF 2** (Figure S8). For VF2.1.Cl, we observe a small increase in cAPD values, which was not statistically significant (Figure S8). Together, these results suggest that **fVF 2** has a phototoxicity that is lower than that of VF2.1.Cl and can be used to measure activity in cardiomyocyte monolayers for prolonged periods of time. Previous reports note slight differences in the structure of transmembrane probes can explain differences in phototoxicity.[38] Experiments are underway to probe the precise molecular mechanisms underlying the faster photobleaching but reduced phototoxicity of **fVF 2** compared to that of VF2.1.Cl.

To assess the ability of **fVF 2** to measure changes to cardiac electrophysiology in response to chronic drug treatment, we calculated IC_{50} values for cisapride using in-well dose escalation with optical recording of cAPD. Measurements were taken after incubation with increasing cisapride concentrations in each well from 0.1 to 300 nM. Our optical measurements show an increase in cAPD90 (IC_{50} = 10.6 nM; 14 days in culture) to 300 nM cisapride (Figure 4e,f), which is in the range of IC_{50} values previously measured for cisapride in other *in vitro* studies (Table S3).[32] We also observe an increase in cAPD50 to 100 nM but a decrease at higher concentrations of cisapride. Similarly, the measured cAPD30 seems to vary little from that of the dimethyl sulfoxide vehicle control; however, a decrease is detected at higher concentrations of cisapride (Figure 4e,f). Together, these results demonstrate the ability to **fVF 2** to enable the rapid assembly of dose−response data in hiSPCs using an all-optical approach.

In summary, we present the design, synthesis, and application of a new class of molecular wire-based fluorescent indicators. We show, for the first time, that fluorene-based molecular wires provide a platform for PeT-based voltage sensing. In general, these fluorene-based indicators have lower

DOI: 10.1021/acschembio.8b00978
ACS Chem. Biol. XXXX, XXX, XXX−XXX

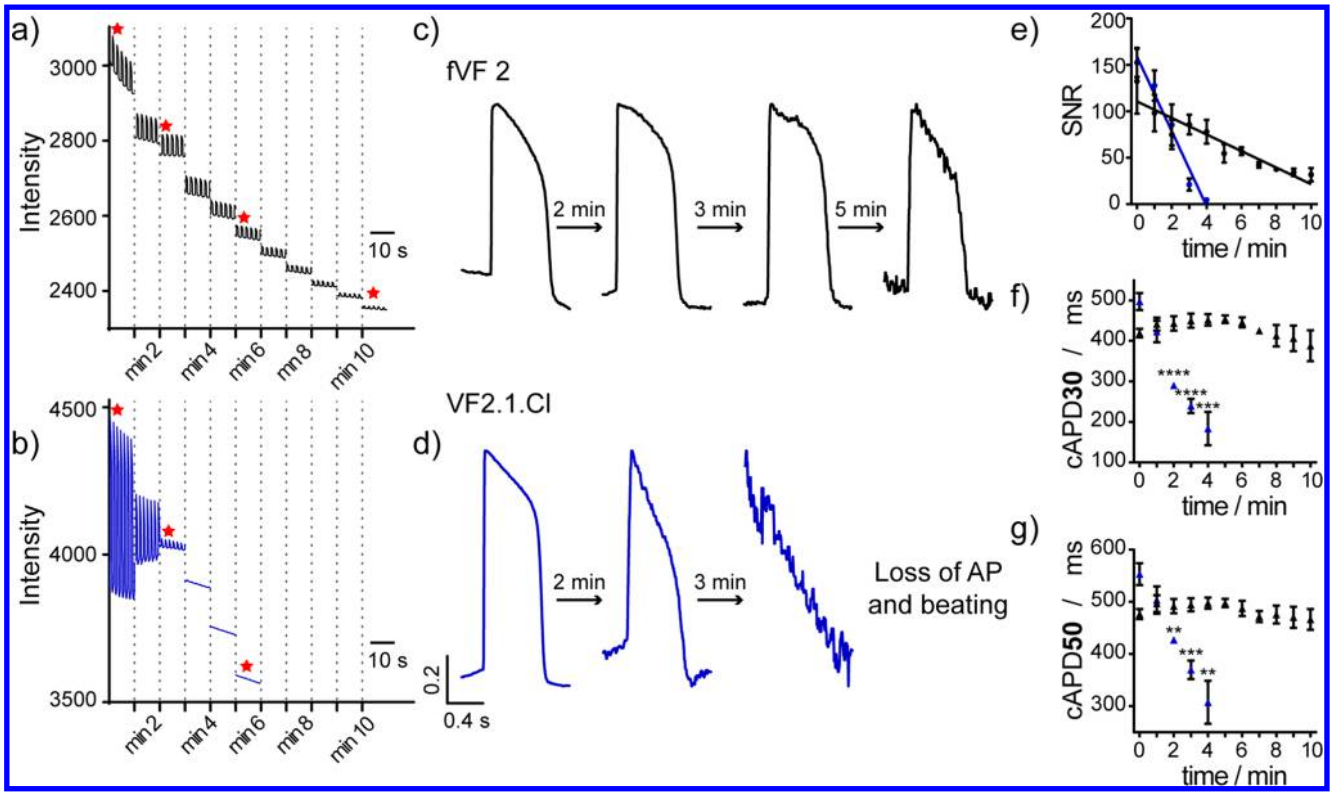

Figure 3. **fVF 2** displays low phototoxicity in cardiomyocyte monolayers. Fluorescence intensity vs time for (a) **fVF 2** and (b) VF2.1.Cl in monolayers of hiSPC-CMs. The raw fluorescence intensity from an entire field of view over an entire 10 s recording session is plotted vs the total illumination time (in minutes). Individual action potential (AP) traces for (c) **fVF 2** and (d) VF2.1.Cl are indicated by red stars in panels a and b. Plot of the mean (e) signal-to-noise ratio (SNR), (f) cAPD30, and (g) cAPD50 as a function of total illumination time for **fVF 2** (black) and VF2.1.Cl (blue). For panels e–g, mean values are determined from $n = 3$ independent trials, and error bars are ±standard error of the mean. Statistical tests were two-tailed, unpaired t tests for each cAPD at the indicated time vs time zero. $^{**}p < 0.005$. $^{***}p < 0.001$. $^{****}p < 0.0001$.

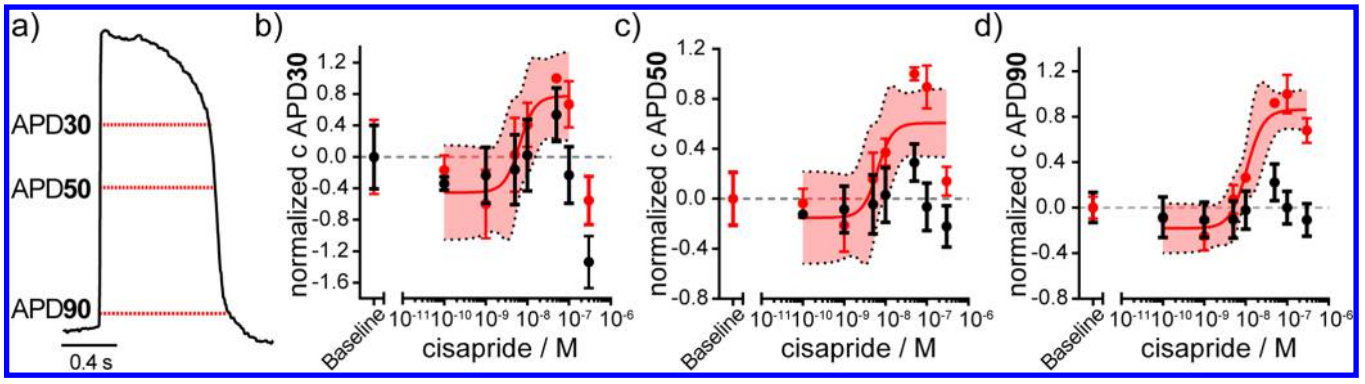

Figure 4. Fluorene VoltageFluor 2 (**fVF 2**) reveals changes to cardiac action potentials (APs) upon treatment with cisapride. (a) Action potential duration (APD) values calculated from the maximum derivative of the depolarization to the repolarization at 70, 50, and 10% of the maximum depolarization value are corrected for beat rate and reported as cAPD30, cAPD50, and cAPD90, respectively. Treatment of monolayers cultured for 14 days with doses of cisapride from 0.1 to 300 nM (red) results in (b) little change in cAPD30, (c) a moderate increase in cAPD50, and (d) a clear increase in cAPD90. Black points indicate data for dimethyl sulfoxide-treated control samples. Plots indicate mean values ± the standard error of the mean for $n = 4$ independent experiments.

nominal voltage sensitivities ($\Delta F/F$ per 100 mV of 5–13% in HEK cells, compared to approximately 27% for VF2.1.Cl) to changes in membrane potential but are brighter than their phenylene-vinylene counterparts. **fVF 2** exhibits adequate sensitivity and excellent brightness in cells for reporting AP waveforms in neurons and cardiomyocytes with high SNRs. More importantly, **fVF 2** displays a substantially reduced phototoxicity in cardiomyocytes relative to that of VF2.1.Cl, allowing for prolonged, continuous measurement of cardiomyocyte activity. Fluorene-based molecular wires may provide an attractive, general solution to the phototoxicity often associated with voltage-sensitive fluorescent indicators.

■ ASSOCIATED CONTENT

Supporting Information

The Supporting Information is available free of charge on the ACS Publications website at DOI: 10.1021/acschembio.8b00978.

DOI: 10.1021/acschembio.8b00978
ACS Chem. Biol. XXXX, XXX, XXX–XXX

Experimental details, synthetic procedures, imaging conditions, cell culture and differentiation protocols, and supporting figures (PDF)

AUTHOR INFORMATION

Corresponding Author

*E-mail: evanwmiller@berkeley.edu.

ORCID

Kevin E. Healy: 0000-0002-8524-3671

Evan W. Miller: 0000-0002-6556-7679

Present Address

#N.H.: Department of Biomedical Engineering, Washington University in St. Louis, St. Louis, Missouri 63130.

Notes

The authors declare no competing financial interest.

ACKNOWLEDGMENTS

The authors gratefully acknowledge financial support of this research from the following organizations: National Institutes of Health, Grants R35GM119855 (E.W.M.), T32GM066698 (S.C.B.), and R01HL130417 (K.E.H.); and the California Institute for Regenerative Medicine (Grant DISC2-100090 to K.E.H.).

REFERENCES

(1) Tsien, R. Y. (2005) Building and Breeding Molecules to Spy on Cells and Tumors. *FEBS Lett. 579*, 927−932.

(2) Yun, S.-W., Kang, N.-Y., Park, S.-J., Ha, H.-H., Kim, Y. K., Lee, J.-S., and Chang, Y.-T. (2014) Diversity Oriented Fluorescence Library Approach (Dofla) for Live Cell Imaging Probe Development. *Acc. Chem. Res. 47*, 1277−1286.

(3) Lavis, L. D. (2017) Teaching Old Dyes New Tricks: Biological Probes Built from Fluoresceins and Rhodamines. *Annu. Rev. Biochem. 86*, 825−843.

(4) Klymchenko, A. S. (2017) Solvatochromic and Fluorogenic Dyes as Environment-Sensitive Probes: Design and Biological Applications. *Acc. Chem. Res. 50*, 366−375.

(5) Dal Molin, M., Verolet, Q., Colom, A., Letrun, R., Derivery, E., Gonzalez-Gaitan, M., Vauthey, E., Roux, A., Sakai, N., and Matile, S. (2015) Fluorescent Flippers for Mechanosensitive Membrane Probes. *J. Am. Chem. Soc. 137*, 568−571.

(6) Peterka, D. S., Takahashi, H., and Yuste, R. (2011) Imaging Voltage in Neurons. *Neuron 69*, 9−21.

(7) Miller, E. W., Lin, J. Y., Frady, E. P., Steinbach, P. A., Kristan, W. B., and Tsien, R. Y. (2012) Optically Monitoring Voltage in Neurons by Photo-Induced Electron Transfer through Molecular Wires. *Proc. Natl. Acad. Sci. U. S. A. 109*, 2114−2119.

(8) Miller, E. W. (2016) Small Molecule Fluorescent Voltage Indicators for Studying Membrane Potential. *Curr. Opin. Chem. Biol. 33*, 74−80.

(9) Deal, P. E., Kulkarni, R. U., Al-Abdullatif, S. H., and Miller, E. W. (2016) Isomerically Pure Tetramethylrhodamine Voltage Reporters. *J. Am. Chem. Soc. 138*, 9085−9088.

(10) Huang, Y. L., Walker, A. S., and Miller, E. W. (2015) A Photostable Silicon Rhodamine Platform for Optical Voltage Sensing. *J. Am. Chem. Soc. 137*, 10767−10776.

(11) Davis, W. B., Svec, W. A., Ratner, M. A., and Wasielewski, M. R. (1998) Molecular-Wire Behaviour in P-Phenylenevinylene Oligomers. *Nature 396*, 60−63.

(12) Pourtois, G., Beljonne, D., Cornil, J., Ratner, M. a., and Brédas, J. L. (2002) Photoinduced Electron-Transfer Processes Along Molecular Wires Based on Phenylenevinylene Oligomers: A Quantum-Chemical Insight. *J. Am. Chem. Soc. 124*, 4436−4447.

(13) Woodford, C. R., Frady, E. P., Smith, R. S., Morey, B., Canzi, G., Palida, S. F., Araneda, R. C., Kristan, W. B., Kubiak, C. P., Miller, E. W., and Tsien, R. Y. (2015) Improved Pet Molecules for Optically Sensing Voltage in Neurons. *J. Am. Chem. Soc. 137*, 1817−1824.

(14) Goldsmith, R. H., Sinks, L. E., Kelley, R. F., Betzen, L. J., Liu, W. H., Weiss, E. A., Ratner, M. A., and Wasielewski, M. R. (2005) Wire-Like Charge Transport at near Constant Bridge Energy through Fluorene Oligomers. *Proc. Natl. Acad. Sci. U. S. A. 102*, 3540−3545.

(15) Eng, M. P., and Albinsson, B. (2006) Non-Exponential Distance Dependence of Bridge-Mediated Electronic Coupling. *Angew. Chem., Int. Ed. 45*, 5626−5629.

(16) Albinsson, B., and Martensson, J. (2008) Long-Range Electron and Excitation Energy Transfer in Donor-Bridge-Acceptor Systems. *J. Photochem. Photobiol., C 9*, 138−155.

(17) Nacci, C., Viertel, A., Hecht, S., and Grill, L. (2016) Covalent Assembly and Characterization of Nonsymmetrical Single-Molecule Nodes. *Angew. Chem., Int. Ed. 55*, 13724−13728.

(18) Kleeberg, C., Dang, L., Lin, Z., and Marder, T. B. (2009) A Facile Route to Aryl Boronates: Room-Temperature, Copper-Catalyzed Borylation of Aryl Halides with Alkoxy Diboron Reagents. *Angew. Chem., Int. Ed. 48*, 5350−5354.

(19) Sager, P. T., Gintant, G., Turner, J. R., Pettit, S., and Stockbridge, N. (2014) Rechanneling the Cardiac Proarrhythmia Safety Paradigm: A Meeting Report from the Cardiac Safety Research Consortium. *Am. Heart J. 167*, 292−300.

(20) Colatsky, T., Fermini, B., Gintant, G., Pierson, J. B., Sager, P., Sekino, Y., Strauss, D. G., and Stockbridge, N. (2016) The Comprehensive in Vitro Proarrhythmia Assay (Cipa) Initiative — Update on Progress. *J. Pharmacol. Toxicol. Methods 81*, 15−20.

(21) Mathur, A., Loskill, P., Shao, K., Huebsch, N., Hong, S., Marcus, S. G., Marks, N., Mandegar, M., Conklin, B. R., Lee, L. P., and Healy, K. E. (2015) Human Ipsc-Based Cardiac Microphysiological System for Drug Screening Applications. *Sci. Rep. 5*, 8883.

(22) Lian, X. J., Hsiao, C., Wilson, G., Zhu, K. X., Hazeltine, L. B., Azarin, S. M., Raval, K. K., Zhang, J. H., Kamp, T. J., and Palecek, S. P. (2012) Robust Cardiomyocyte Differentiation from Human Pluripotent Stem Cells Via Temporal Modulation of Canonical Wnt Signaling. *Proc. Natl. Acad. Sci. U. S. A. 109*, E1848−E1857.

(23) Ma, Z., Wang, J., Loskill, P., Huebsch, N., Koo, S., Svedlund, F. L., Marks, N. C., Hua, E. W., Grigoropoulos, C. P., Conklin, B. R., and Healy, K. E. (2015) Self-Organizing Human Cardiac Microchambers Mediated by Geometric Confinement. *Nat. Commun. 6*, 7413.

(24) Huebsch, N., Loskill, P., Deveshwar, N., Spencer, C. I., Judge, L. M., Mandegar, M. A., Fox, C. B., Mohamed, T. M. A., Ma, Z., Mathur, A., Sheehan, A. M., Truong, A., Saxton, M., Yoo, J., Srivastava, D., Desai, T. A., So, P. L., Healy, K. E., and Conklin, B. R. (2016) Miniaturized Ips-Cell-Derived Cardiac Muscles for Physiologically Relevant Drug Response Analyses. *Sci. Rep. 6*, 24726.

(25) Ma, Z., Huebsch, N., Koo, S., Mandegar, M. A., Siemons, B., Boggess, S., Conklin, B. R., Grigoropoulos, C. P., and Healy, K. E. (2018) Contractile Deficits in Engineered Cardiac Microtissues as a Result of Mybpc3 Deficiency and Mechanical Overload. *Nature Biomedical Engineering 2*, 955.

(26) Laughner, J. I., Ng, F. S., Sulkin, M. S., Arthur, R. M., and Efimov, I. R. (2012) Processing and Analysis of Cardiac Optical Mapping Data Obtained with Potentiometric Dyes. *Am. J. Phys. Heart Circ Physiol 303*, H753−765.

(27) Dempsey, G. T., Chaudhary, K. W., Atwater, N., Nguyen, C., Brown, B. S., McNeish, J. D., Cohen, A. E., and Kralj, J. M. (2016) Cardiotoxicity Screening with Simultaneous Optogenetic Pacing, Voltage Imaging and Calcium Imaging. *J. Pharmacol. Toxicol. Methods 81*, 240−250.

(28) Lu, H. R., Hortigon-Vinagre, M. P., Zamora, V., Kopljar, I., De Bondt, A., Gallacher, D. J., and Smith, G. (2017) Application of Optical Action Potentials in Human Induced Pluripotent Stem Cells-Derived Cardiomyocytes to Predict Drug-Induced Cardiac Arrhythmias. *J. Pharmacol. Toxicol. Methods 87*, 53−67.

(29) Luo, S., Michler, K., Johnston, P., and Macfarlane, P. W. (2004) A Comparison of Commonly Used Qt Correction Formulae: The

DOI: 10.1021/acschembio.8b00978
ACS Chem. Biol. XXXX, XXX, XXX−XXX

Effect of Heart Rate on the Qtc of Normal Ecgs. *J. Electrocardiol 37* (Suppl), 81−90.
(30) Itzhaki, I., Maizels, L., Huber, I., Zwi-Dantsis, L., Caspi, O., Winterstern, A., Feldman, O., Gepstein, A., Arbel, G., Hammerman, H., Boulos, M., and Gepstein, L. (2011) Modelling the Long Qt Syndrome with Induced Pluripotent Stem Cells. *Nature 471*, 225−229.
(31) Caspi, O., Itzhaki, I., Kehat, I., Gepstein, A., Arbel, G., Huber, I., Satin, J., and Gepstein, L. (2009) In Vitro Electrophysiological Drug Testing Using Human Embryonic Stem Cell Derived Cardiomyocytes. *Stem Cells Dev. 18*, 161−172.
(32) Crumb, W. J., Vicente, J., Johannesen, L., and Strauss, D. G. (2016) An Evaluation of 30 Clinical Drugs against the Comprehensive in Vitro Proarrhythmia Assay (Cipa) Proposed Ion Channel Panel. *J. Pharmacol. Toxicol. Methods 81*, 251−262.
(33) Redfern, W. S., Carlsson, L., Davis, A. S., Lynch, W. G., MacKenzie, I., Palethorpe, S., Siegl, P. K. S., Strang, I., Sullivan, A. T., Wallis, R., Camm, A. J., and Hammond, T. G. (2003) Relationships between Preclinical Cardiac Electrophysiology, Clinical Qt Interval Prolongation and Torsade De Pointes for a Broad Range of Drugs: Evidence for a Provisional Safety Margin in Drug Development. *Cardiovasc. Res. 58*, 32−45.
(34) Harris, K., Aylott, M., Cui, Y., Louttit, J. B., McMahon, N. C., and Sridhar, A. (2013) Comparison of Electrophysiological Data from Human-Induced Pluripotent Stem Cell-Derived Cardiomyocytes to Functional Preclinical Safety Assays. *Toxicol. Sci. 134*, 412−426.
(35) McKeithan, W. L., Savchenko, A., Yu, M. S., Cerignoli, F., Bruyneel, A. A. N., Price, J. H., Colas, A. R., Miller, E. W., Cashman, J. R., and Mercola, M. (2017) An Automated Platform for Assessment of Congenital and Drug-Induced Arrhythmia with Hipsc-Derived Cardiomyocytes. *Front. Physiol. 8*, 766.
(36) Bedut, S., Seminatore-Nole, C., Lamamy, V., Caignard, S., Boutin, J. A., Nosjean, O., Stephan, J.-P., and Coge, F. (2016) High-Throughput Drug Profiling with Voltage- and Calcium-Sensitive Fluorescent Probes in Human Ipsc-Derived Cardiomyocytes. *Am. J. Phys. Heart Circ Physiol 311*, H44−H53.
(37) McPheeters, M. T., Wang, Y. T., Werdich, A. A., Jenkins, M. W., and Laurita, K. R. (2017) An Infrared Optical Pacing System for Screening Cardiac Electrophysiology in Human Cardiomyocytes. *PLoS One 12*, e0183761.
(38) Rohr, S., and Salzberg, B. M. (1994) Multiple Site Optical Recording of Transmembrane Voltage (Msortv) in Patterned Growth Heart Cell Cultures: Assessing Electrical Behavior, with Microsecond Resolution, on a Cellular and Subcellular Scale. *Biophys. J. 67*, 1301−1315.

DOI: 10.1021/acschembio.8b00978
ACS Chem. Biol. XXXX, XXX, XXX−XXX